

# Extending the Numerical Flow Iteration to the multi-species Vlasov–Maxwell system through Hamiltonian Splitting

R.-Paul Wilhelm<sup>1,2</sup>, Fabio Bacchini<sup>1,5</sup>, Sebastian Schöps<sup>3</sup>,  
Manuel Torrilhon<sup>2</sup>, Melina Merkel<sup>3</sup>, Matthias Kirchhart<sup>2,4</sup>

November 14, 2025

## Abstract

The Numerical Flow Iteration (NuFI) method has recently been proposed as a memory-slim solution method for the Vlasov–Poisson system. It stores the temporal evolution of the electric field, instead of the distribution functions, and reconstructs the solution in each time step by following the characteristics backwards in time and reconstructing the solution from the initial distribution. NuFI has been shown to be more accurate than other state-of-the-art Vlasov solvers given the same amount of degrees of freedom as well as interpolation order, essentially making NuFI a high-fidelity but low-memory cost scheme. In this paper, we build on the Hamiltonian structure of the full Vlasov–Maxwell system to extend NuFI to handle electro-magnetic kinetic plasma dynamics. We show that the advanced structure-preserving properties of NuFI are preserved when extending to the electro-magnetic case.

Keywords: Plasma Physics, Kinetic Theory, Vlasov equation, Maxwell’s equation, Numerical Methods

## 1. Introduction

In many applications such as nuclear fusion devices or solar wind it is relevant to fundamentally understand how turbulence and instabilities in a plasma are triggered and how they evolve over time. Some phenomena can already be observed through a fluid-description but when plasma becomes rarefied or hot the velocity distribution of the charged particles can substantially deviate from equilibrium, which breaks the fundamental assumption of a fluid-descriptions. In this

---

<sup>1</sup>Centre for mathematical Plasma Astrophysics (CmPA), KU Leuven, Belgium.

<sup>2</sup>Institute for Applied and Computational Mathematics (ACoM), RWTH Aachen University.

<sup>3</sup>Institute for Accelerator Science and Electromagnetic Fields (TEMF), TU Darmstadt.

<sup>4</sup>Nvidia GmbH, Munich.

<sup>5</sup>Royal Belgian Institute for Space Aeronomy, Brussels, Belgium

case one has to model the plasma evolution through kinetic theory, i.e., including the velocity distributions in the model, which results in the Vlasov equation<sup>[1]</sup>

$$\partial_t f^\alpha + \mathbf{v} \cdot \nabla_{\mathbf{x}} f^\alpha + \frac{q_\alpha}{m_\alpha} (\mathbf{E} + \mathbf{v} \times \mathbf{B}) \cdot \nabla_{\mathbf{v}} f^\alpha = 0. \quad (1)$$

where  $f^\alpha : [0, +\infty) \times \mathbb{R}^d \times \mathbb{R}^d \rightarrow [0, +\infty)$  is the probability distribution of the species  $\alpha$  in the up to six-dimensional phase-space and  $\mathbf{E} : [0, +\infty) \times \mathbb{R}^d \rightarrow \mathbb{R}^d$  and  $\mathbf{B} : [0, +\infty) \times \mathbb{R}^d \rightarrow \mathbb{R}^d$  are the self-induced electro-magnetic forces acting upon the species  $\alpha$ . The Vlasov equation is coupled to the Maxwell's equations

$$\nabla \times \mathbf{E} + \partial_t \mathbf{B} = 0, \quad (2)$$

$$\nabla \times \mathbf{B} - \partial_t \mathbf{E} = \mathbf{j}, \quad (3)$$

$$\nabla \cdot \mathbf{E} = \rho, \quad (4)$$

$$\nabla \cdot \mathbf{B} = 0. \quad (5)$$

The right hand side of the Maxwell's equations is computed from the phase-space distribution functions  $f^\alpha$ :

$$\rho(t, \mathbf{x}) = \sum_\alpha \rho^\alpha(t, \mathbf{x}) = \sum_\alpha \int_{\mathbb{R}^d} f^\alpha(t, \mathbf{x}, \mathbf{v}) d\mathbf{v}, \quad (6)$$

$$\mathbf{j}(t, \mathbf{x}) = \sum_\alpha \mathbf{j}^\alpha(t, \mathbf{x}) = \sum_\alpha \int_{\mathbb{R}^d} \mathbf{v} f^\alpha(t, \mathbf{x}, \mathbf{v}) d\mathbf{v}. \quad (7)$$

With this coupling equations (1) – (7) become the (non-linear) Vlasov–Maxwell system. We use the normalized version of the Vlasov–Maxwell system in rationalized Gaussian units following Morrison,<sup>[2]</sup> details can be found in appendix A.

Solving the Vlasov system poses a number of significant challenges: The solution lives in the six-dimensional phase-space inducing the curse of dimensionality for methods trying to directly discretize the distribution function. Hence to simulate the full system one either either has to use low resolution or reduce the system size with a number of additional assumptions on the physics to reduce the dimension of phase space. Additionally, kinetic plasma dynamics are commonly only weakly collisional or, in the version we use in this paper (1), entirely collisionless, which is a reasonable assumption in many astrophysical settings.<sup>[1],[3],[4]</sup> Therefore the physics lack a (strong) mechanism to dissipate fine structures in the distribution function and, due to the non-linearity of the system, fine scale structures—often referred to as filaments—develop and remain in the distribution function over long time-scales. The filamentation has to be resolved to accurately capture the onset of some instabilities and there is some evidence that they play a key role in the heat dissipation in a plasma.<sup>[3],[5],[6]</sup> However, resolving these fine scale structures also requires the use of (prohibitively) high resolutions. Finally, due to the large mass difference between electrons and ions, the dynamics of multi-species plasma systems are also inherently multi-scale, requiring even higher resolutions if we are interested in all scales.<sup>[3]</sup>

Numerical solvers for the Vlasov equation can generally be grouped into three main classes: Eulerian (or Discrete Velocity), Semi-Lagrangian, and Lagrangian schemes. Both Eulerian and Semi-Lagrangian approaches are grid-based, meaning that the distribution function  $f$  is represented on a discrete phase-space grid. Their distinction lies primarily in how they advance the solution in time. In Eulerian schemes, the grid values are updated by evaluating the local temporal rate of change, effectively rewriting the Vlasov equation as a large system of ordinary differential equations (ODEs)—one for each degree of freedom in the discretization.<sup>[7],[8],[9],[10],[11],[12],[13],[14],[15],[16]</sup>

Although Eulerian methods are widely used in fluid dynamics, their application to kinetic equations such as the Vlasov equation is less common. The Eulerian framework offers a general methodology for formulating numerical solvers for PDEs, yet it typically neglects the intrinsic structural properties of the underlying physical system.

The Semi-Lagrangian method also represents the distribution function on a phase-space grid, but its evolution differs fundamentally from the Eulerian approach. Here, each grid point is traced backwards in time over a short interval by integrating the characteristic equations. The new-time solution is then obtained by interpolating from the previous time step, evaluating  $f$  at the foot of the characteristic.<sup>1</sup> This procedure enhances the conservation properties compared to purely Eulerian methods, particularly, when coupled with a symplectic time integrator, and also removes the CFL time-step restriction that limits Eulerian schemes.<sup>[17]</sup> A popular choice for interpolation is the use of (cubic) B-splines, which provide an effective balance between accuracy and computational cost.<sup>[18],[19]</sup> Other implementations instead rely on nodal interpolation methods.<sup>[20],[21],[22],[23],[24],[25],[26],[27],[28]</sup> Despite their advantages, grid-based Vlasov solvers face serious challenges. The curse of dimensionality makes storing and updating a full six-dimensional grid extremely costly, especially when adaptive resolution or non-rectangular geometries are needed. The large memory footprint also causes significant communication overhead, reducing parallel efficiency and scalability on modern accelerator architectures.<sup>[19],[29],[30],[31]</sup> Incorporating sparse-grid techniques or adaptive meshes is particularly difficult in such high dimensions.<sup>[32],[33]</sup> Moreover, discretization on fixed grids inevitably introduces numerical diffusion, which—being an artificial source of dissipation—violates the conservative, collisionless nature of the Vlasov system. Although various strategies aim to reduce this effect, it remains intrinsic to all grid-based methods.<sup>[13],[21]</sup> Finally, complex domain geometries, boundary conditions, and expanding velocity supports pose additional difficulties for grid-based formulations.<sup>[34],[35],[36]</sup>

An alternative to grid-based discretizations is to employ particle-based, or Lagrangian, solvers. The most widely used example is the Particle-In-Cell (PIC) method, though other particle approaches exist, such as Smoothed Particle Hydrodynamics (SPH) and the Reproducing Kernel Hilbert Space Particle Method (RKHS-PM).<sup>[37],[38],[39],[40]</sup> In PIC the distribution function is represented by a collection of marker particles, each carrying a value or weight that is transported along the characteristics of the Vlasov equation. Because the particle paths coincide with the characteristics, their associated weights remain constant in time. For PIC a spatial grid is additionally introduced to evaluate and interpolate the electromagnetic fields. The right hand side for the Maxwell equations is obtained by evaluating the charge and current densities on this grid (called charge deposition). The simplest deposition strategy counts the number of particles per cell, but more accurate methods assign shape functions to particles, enabling higher-order charge deposition.<sup>[41],[42],[43],[44],[45]</sup> Although PIC methods still face the curse of dimensionality, they offer several advantages over grid-based schemes. Particles naturally follow the plasma flow, providing automatic adaptivity to the evolving distribution. Moreover, since the data is unstructured, PIC can more easily handle complex geometries, boundary conditions, and distributed parallelization. The main drawback of particle-based representations, however, is the presence of statistical noise. Achieving a given level of accuracy often requires significantly more particles than grid points in deterministic solvers. This issue becomes particularly severe in low-density regions or when high accuracy is required. Most PIC implementations are explicit in time,<sup>[46],[47],[48],[49],[50],[51]</sup> i. e., where the field and particle updates are performed using explicit time integration. Because

---

<sup>1</sup>The approach described here is a backward Semi-Lagrangian (BSL) scheme. Propagating grid points forward in time instead leads to a forward Semi-Lagrangian (FSL) variant. In the following, we use Semi-Lagrangian to refer specifically to the BSL formulation unless stated otherwise.

plasma dynamics are inherently multi-scale, due to the large mass disparity between electrons and ions as well as the system size, explicit PIC schemes often demand very fine temporal and spatial resolutions to capture all relevant physics. To address this, various semi-implicit and fully implicit formulations have been developed, which relax the stringent stability and resolution constraints of explicit methods.<sup>[52],[53],[54],[55],[56],[57],[58],[59],[60]</sup>

A more detailed overview of numerical solvers for the Vlasov equation can be found in e.g. the reviews by Filbet and Sonnendrücker<sup>[61]</sup> or, more recently, Palmroth et al.<sup>[36]</sup>

Recently a new class of schemes was introduced to approximate the flow map of the Vlasov equation instead of the distribution function, whereby one tries to further preserve the Lagrangian structure of the Vlasov system. The two main approaches in this direction are the Characteristic Mapping Method (CMM) introduced by Krah et al. [62] and the Numerical Flow Iteration (NuFI) introduced by Kirchhart and Wilhelm<sup>[63]</sup> for the electro-static Vlasov–Poisson system. CMM directly stores the flow map on a phase-space grid and exploits the sub-group property of the flow to compose several sub-maps, which can be stored on a coarser grid than the full map (or distribution function), and thereby can achieve good sub-grid resolution. However, CMM does not exactly preserve the conservation properties of the Vlasov system as the time stepping is not symplectic. In contrast to this, NuFI employs an iterative-in-time approximation of the characteristics based on symplectic operator splitting for the time- integration. This avoids the need of directly discretizing and storing the distribution function, only requiring to store the time-evolution of the electric potentials, while using the symplectic time-stepping scheme leads to preservation of the conservation properties of the analytic solution either analytically in the case of the  $L^p$ -norms and entropy or up to the time-discretization error in the case of the total energy.<sup>2</sup> It has been shown that the structure-preservation of NuFI leads to substantially better results than for Semi-Lagrangian or PIC schemes with comparable resolution and interpolation order. Additionally, because NuFI only looks at the characteristics instead of a fixed discretization of the distribution function in phase-space, it is possible, on the one hand, to zoom into the distribution function in regions of interest (e.g. for post- processing) without having to rerun with higher resolution, and, on the other hand, allows easy introduction of adaptivity and handling of boundary conditions.<sup>[4],[64]</sup> Thus the goal of this paper is to extend NuFI to the fully electro-magnetic case and show that the structure-preservation properties are preserved even in the electro-magnetic case.

In the following, in section 2.1 we will briefly introduce the Numerical Flow Iteration for the electro-static case. Then in section 2.2 we revisit the Hamiltonian of the Vlasov–Maxwell system as well as the associated Hamiltonian splitting. In the sections 2.3 as well as 2.4 we introduce two ways to extend NuFI to the electro-magnetic case using the Hamiltonian splitting and in section 2.5 how the computational complexity of the approach can be reduced. Finally, in section 3 we look at numerical benchmarks to test the extension of NuFI to the Vlasov–Maxwell system.

## 2. Hamiltonian structure of the Vlasov system

### 2.1. The Numerical Flow Iteration in the electro-static case

Before we move on to the fully electro-magnetic case of the Vlasov–Maxwell system, we briefly recap the ideas behind the Numerical Flow Iteration in the simplified electro-static case. If  $|\mathbf{B}| \ll |\mathbf{E}|$ , we can neglect the influence of the magnetic field on the overall dynamics of the

---

<sup>2</sup>There are also Semi-Lagrangian schemes which preserve some subset of these conservation properties, however, in these cases the non-preserved quantities start exhibiting drift over long time-periods due to numerical diffusion introduced by grid-based schemes.

Vlasov–Maxwell system. This in turn allows us to simplify it to the electro-static Vlasov–Poisson system, where the Maxwell equations reduce to the Gauss law, which can be reformulated to a simple Poisson equation for the electro-static potential

$$-\Delta_{\mathbf{x}}\varphi = \rho \quad (8)$$

from which we get the electric field through

$$\mathbf{E} = -\nabla_{\mathbf{x}}\varphi. \quad (9)$$

The Vlasov–Poisson system is a Hamiltonian system with the Hamiltonian

$$\begin{aligned} \mathcal{H}_{VP} &= \mathcal{H}_{\mathbf{E}} + \mathcal{H}_f \\ &= \frac{1}{2} \int_{\mathbb{R}^d} \mathbf{E}^2 d\mathbf{x} + \frac{1}{2} \sum_{\alpha} \int_{\mathbb{R}^d \times \mathbb{R}^d} f^{\alpha} d\mathbf{x} d\mathbf{v}. \end{aligned} \quad (10)$$

This allows us to use operator splitting techniques for time-stepping, i. e., solve the associated characteristic equations through splitting the non-linear Vlasov equation into two linear advection equations associated to the  $\mathcal{H}_{\mathbf{E}}$  and  $\mathcal{H}_f$  respectively. Using the well-known Störmer–Verlet splitting this results in the following scheme: Starting from  $\hat{\mathbf{x}}_n^h = \mathbf{x}$  and  $\hat{\mathbf{v}}_n^h = \mathbf{v}$  at the time-step  $t = t_n$  compute

$$\hat{\mathbf{v}}_{i-1/2}^h = \hat{\mathbf{v}}_i^h - \frac{\Delta t}{2} \frac{q^{\alpha}}{m^{\alpha}} \mathbf{E}(t_i, \hat{\mathbf{x}}_i^{h,\alpha}), \quad (11)$$

$$\hat{\mathbf{x}}_{i-1}^h = \hat{\mathbf{x}}_i^h - \hat{\mathbf{v}}_{i-1/2}^h, \quad (12)$$

$$\hat{\mathbf{v}}_{i-1}^h = \hat{\mathbf{v}}_{i-1/2}^h - \frac{\Delta t}{2} \frac{q^{\alpha}}{m^{\alpha}} \mathbf{E}(t_{i-1}, \hat{\mathbf{x}}_{i-1}^h) \quad (13)$$

for  $i = 0, \dots, n$ .

This operator splitting is widely used in Semi-Lagrangian codes<sup>3</sup> to either advance the characteristics or trace them backwards in time for 1 time-step after which the results can be interpolated and stored on a phase-space grid. The idea behind NuFI is to avoid the phase-space grid altogether and instead use the same scheme (11) – (13) to iterate backwards to the initial time, where one can evaluate the initial data – often prescribed in a closed, analytic form – through the following expression

$$f^{\alpha}(t, \mathbf{x}, \mathbf{v}) = f_0^{\alpha}(\hat{\mathbf{x}}_0^h, \hat{\mathbf{v}}_0^h) + \mathcal{O}(\Delta t^2). \quad (14)$$

Only knowledge of the evolution in time of the electric field is required to evaluate any distribution function  $f^{\alpha}$  at any arbitrary position in phase-space. Therefore – using some numerical quadrature rule – we can integrate (6) to obtain the right-hand side of (8) and combining with a Poisson solver we arrive at a numerical solver for the non-linear Vlasov–Poisson system. A more in detail derivation can be found in the previous works of Wilhelm et al.<sup>[4],[63],[64]</sup>

The advantages of the NuFI approach compared to a classic Semi-Lagrangian scheme are two-fold:

First, instead of storing a 6-dimensional distribution function  $f^{\alpha}$  per species, one only has to store the evolution of the 3-dimensional electric potential  $\varphi$ , i. e., one 4-dimensional instead of several 6-dimensional functions. Additionally, the electric potential is substantially smoother than the individual distribution functions as one has to take the 2nd derivative of  $\varphi$  to obtain  $\rho$ ,

---

<sup>3</sup>The same operator splitting idea is also used in Particle-In-Cell codes where it is often referred to as *Leapfrog* time-integration.

which in turn is obtained by integrating over  $f^\alpha$ . Hence we need less (spatial) degrees of freedom to accurately resolve  $\varphi$ .

Secondly, because the Störmer–Verlet time-integration scheme is symplectic NuFI preserves the conservation properties of the analytic solution. In fact, all  $L^p$ -norms as well as the entropy are preserved analytically while the total energy is preserved up to the discretization error, however, without a drift. Therefore NuFI is structure-preserving far beyond what conventional Semi-Lagrangian schemes for the Vlasov–Poisson system can achieve and, in practice, this manifests through substantially improved accuracy for comparable numerical resolutions.

However, the main disadvantage of NuFI compared to conventional approaches is the increased computational complexity: Because the characteristics are now traced until  $t = 0$  (instead of just 1 time-step) the computational complexity becomes quadratic – instead of linear – in the total number of time-steps in a simulation. The increased complexity makes the pure NuFI approach only feasible for short simulation periods.

## 2.2. Hamiltonian of the Vlasov–Maxwell system

The extension of the Störmer–Verlet-based NuFI scheme from the electro- static to the fully electro-magnetic Vlasov–Maxwell system is not straight forward, if we want to retain the structure-preserving properties of NuFI, and requires us to revisit Hamiltonian structure of the full Vlasov system. The Vlasov–Maxwell system is also a Hamiltonian system with the Hamiltonian being<sup>[2],[65],[66]</sup>

$$\begin{aligned} \mathcal{H}_{VM} &= \mathcal{H}_E &+ \mathcal{H}_B &+ \mathcal{H}_f \\ &= \frac{1}{2} \int_{\mathbb{R}^d} \mathbf{E}^2 d\mathbf{x} &+ \frac{1}{2} \int_{\mathbb{R}^d} \mathbf{B}^2 d\mathbf{x} &+ \frac{1}{2} \sum_{\alpha} \int_{\mathbb{R}^d \times \mathbb{R}^d} f^\alpha d\mathbf{x} d\mathbf{v}. \end{aligned} \quad (15)$$

The three terms  $\mathcal{H}_E$ ,  $\mathcal{H}_B$  and  $\mathcal{H}_f$  correspond to the electric, magnetic and kinetic energy respectively. Assuming that the solution of the system exists and is smooth enough, we can follow the reasoning of Crouseilles et al.<sup>[66]</sup> to derive (linear) partial differential equations associated with each of the sub-Hamiltonians.

### 2.2.1. Equations for $\mathcal{H}_E$

The equations associated to the electric field Hamiltonian  $\mathcal{H}_E$  are

$$\partial_t f^\alpha + \mathbf{E} \cdot \nabla_{\mathbf{v}} f^\alpha = 0, \quad (16)$$

$$\partial_t \mathbf{E} = 0, \quad (17)$$

$$\partial_t \mathbf{B} = -\nabla_{\mathbf{x}} \times \mathbf{E}. \quad (18)$$

Provided the initial data  $\mathbf{E}_0$ ,  $\mathbf{B}_0$  and  $f_0$  at time  $t = 0$  the solution of this linear transport equation can be explicitly stated as

$$f^\alpha(t, \mathbf{x}, \mathbf{v}) = f_0^\alpha(\mathbf{x}, \mathbf{v} - t\mathbf{E}_0(\mathbf{x})), \quad (19)$$

$$\mathbf{E}(t, \mathbf{x}) = \mathbf{E}_0(\mathbf{x}), \quad (20)$$

$$\mathbf{B}(t, \mathbf{x}) = \mathbf{B}_0(\mathbf{x}) - t\nabla_{\mathbf{x}} \times \mathbf{E}_0(\mathbf{x}). \quad (21)$$

### 2.2.2. Equations for $\mathcal{H}_B$

The equations associated to the electric field Hamiltonian  $\mathcal{H}_E$  are

$$\partial_t f^\alpha + (\mathbf{v} \times \mathbf{B}(\mathbf{x})) \cdot \nabla_{\mathbf{v}} f^\alpha = 0, \quad (22)$$

$$\partial_t \mathbf{E} = \nabla_{\mathbf{x}} \times \mathbf{B}, \quad (23)$$

$$\partial_t \mathbf{B} = 0. \quad (24)$$

The solution can be written as

$$f^\alpha(t, \mathbf{x}, \mathbf{v}) = f_0^\alpha(\mathbf{x}, \exp(-\mathbb{J}_B t) \mathbf{v}), \quad (25)$$

$$\mathbf{E}(t, \mathbf{x}) = \mathbf{E}_0(\mathbf{x}) + t \nabla_{\mathbf{x}} \times \mathbf{B}_0(\mathbf{x}), \quad (26)$$

$$\mathbf{B}(t, \mathbf{x}) = \mathbf{B}_0(\mathbf{x}). \quad (27)$$

Here we used that the cross-product between two vectors  $a, b \in \mathbb{R}^3$  can be rewritten into a vector-matrix product through

$$a \times b = \begin{pmatrix} a_2 b_3 - a_3 b_2 \\ a_3 b_1 - a_1 b_3 \\ a_1 b_2 - a_2 b_1 \end{pmatrix} = \underbrace{\begin{pmatrix} 0 & b_3 & -b_2 \\ -b_3 & 0 & b_1 \\ b_2 & -b_1 & 0 \end{pmatrix}}_{=: \mathbb{J}_b} a. \quad (28)$$

By  $\exp(-\mathbb{J}_B t)$  we denote the natural matrix exponential.

### 2.2.3. Equations for $\mathcal{H}_f$

The equations associated to the electric field Hamiltonian  $\mathcal{H}_E$  are

$$\partial_t f^\alpha + \mathbf{v} \nabla_{\mathbf{x}} f^\alpha = 0, \quad (29)$$

$$\partial_t \mathbf{E} = -\mathbf{j}, \quad (30)$$

$$\partial_t \mathbf{B} = 0. \quad (31)$$

The solution can be written as

$$f^\alpha(t, \mathbf{x}, \mathbf{v}) = f_0^\alpha(\mathbf{x} - t\mathbf{v}, \mathbf{v}), \quad (32)$$

$$\mathbf{E}(t, \mathbf{x}) = \mathbf{E}_0(\mathbf{x}) + \int_0^t \sum_\alpha \left( \int_{\mathbb{R}^3} \mathbf{v} f_0^\alpha(\mathbf{x} - s\mathbf{v}, \mathbf{v}) d\mathbf{v} \right) ds, \quad (33)$$

$$\mathbf{B}(t, \mathbf{x}) = \mathbf{B}_0(\mathbf{x}). \quad (34)$$

Note that (33) can be further rewritten to

$$\begin{aligned} \mathbf{E}(t, \mathbf{x}) &= \mathbf{E}_0(\mathbf{x}) + \int_0^t \sum_\alpha q_\alpha \left( \int_{\mathbb{R}^3} \mathbf{v} f^\alpha(s, \mathbf{x}, \mathbf{v}) d\mathbf{v} \right) ds \\ &= \mathbf{E}_0(\mathbf{x}) + \int_0^t \sum_\alpha \mathbf{j}(s, \mathbf{x}) ds. \end{aligned} \quad (35)$$

**Remark 2.1** Note that the Gauss law for the electric (4) and for the magnetic field (5) are preserved by construction through the solutions of these sub-systems.<sup>[66]</sup>

### 2.3. Numerical Implementation purely through Hamiltonian splitting

Because the resulting sub-systems are all linear transport equations they admit analytic solutions. Therefore, we can use operator-splitting techniques to construct an approximate solution up to splitting error for the Vlasov–Maxwell system.<sup>[66],[67]</sup> Following Crouseilles et al. we first look at the first order in time *Lie splitting* approach choosing the order

$$F(t) = \exp(\mathcal{H}_E) \exp(\mathcal{H}_B) \exp(\mathcal{H}_f) F(0), \quad (36)$$

where we denote the solution triplet as  $F(t) = (f, \mathbf{E}, \mathbf{B})$ .

**Remark 2.2**

1. Higher order splitting schemes, e. g., through Strang splitting are also possible in principle.<sup>[67]</sup> However, we have to keep in mind through the way NuFI is constructed for the Vlasov–Maxwell system higher-order splitting schemes in time also involve evaluation of higher order derivatives in space: Because the analytic solutions (21) and (26) involve a rotation operator, composing the  $\mathcal{H}_E$  and  $\mathcal{H}_B$  operators  $m \in \mathbb{N}$  times requires us to take up to  $m$ th derivatives of the fields. Hence the representation of the fields has to allow us to take higher-order derivatives, i. e., be sufficiently smooth.
2. Note that in (36) other orders of the operators are possible, but we chose the present order such that we minimize the sub- steps required to evaluate  $\hat{\mathbf{j}}$  and thus to reduce the computational load. In section 2.4 we revisit our choice of ordering the operators with regards to stability of the Maxwell update.

To simplify the derivation of the numerical formula, in particular for the fields, we restrict ourselves to the case of periodic boundary conditions. In space we are using B-splines of order  $m \in \mathbb{N}$  on a uniform grid, which naturally allow us to take derivatives of up to order  $m - 1$ .<sup>[63]</sup> For the time discretization we fix a time-step  $\Delta t$ . Assuming that we are given the initial data  $\tilde{f}_0^\alpha$ ,  $\tilde{\mathbf{B}}_0$  and  $\tilde{\mathbf{E}}_0$  (such that they can be pointwise evaluated) we can then derive a numerical scheme by composing the analytic solutions of the linear sub-equations for one time step.

Corresponding to  $\mathcal{H}_f$  we obtain

$$f_1^\alpha(\mathbf{x}, \mathbf{v}) = \tilde{f}_0^\alpha(\mathbf{x} - \Delta t \mathbf{v}, \mathbf{v}), \quad (37)$$

$$\mathbf{B}_1(\mathbf{x}) = \tilde{\mathbf{B}}_0(\mathbf{x}), \quad (38)$$

$$\mathbf{E}_1(\mathbf{x}) = \tilde{\mathbf{E}}_0(\mathbf{x}) - \sum_{\alpha} q_{\alpha} \int_0^{\Delta t} \int_{\mathbb{R}^3} \mathbf{v} \tilde{f}_0^\alpha(\mathbf{x} - s \mathbf{v}, \mathbf{v}) d\mathbf{v} ds. \quad (39)$$

In equation (39) we can approximate the time-integral through a mid-point rule

$$\mathbf{E}_1(\mathbf{x}) = \tilde{\mathbf{E}}_0(\mathbf{x}) - \Delta t \sum_{\alpha} q_{\alpha} \int_{\mathbb{R}^3} \mathbf{v} \tilde{f}_0^\alpha(\mathbf{x} - \frac{\Delta t}{2} \mathbf{v}, \mathbf{v}) d\mathbf{v}. \quad (40)$$

Note that this approximation is also  $\mathcal{O}(\Delta t)$ , i. e., first order in time, same as the chosen Lie splitting. Hence choosing a higher order time-integration would only make sense if we also introduce higher order time splitting. The remaining integral in velocity space is then resolved by a mid-point rule in truncated velocity space:

$$\hat{\mathbf{j}}(\mathbf{x}) := \sum_{\alpha} q_{\alpha} \sum_{i_u=1}^{N_u^\alpha} \sum_{i_v=1}^{N_v^\alpha} \sum_{i_w=1}^{N_w^\alpha} \mathbf{v}_{i_u, i_v, i_w}^{h, \alpha} \tilde{f}_0^\alpha(\mathbf{x} - \frac{\Delta t}{2} \mathbf{v}_{i_u, i_v, i_w}^{h, \alpha}, \mathbf{v}_{i_u, i_v, i_w}^{h, \alpha}), \quad (41)$$

where

$$\mathbf{v}_{i_u, i_v, i_w}^{h, \alpha} = \begin{pmatrix} v_{\min}^{1, \alpha} + (i_u + \frac{1}{2}) \Delta u \\ v_{\min}^{2, \alpha} + (i_v + \frac{1}{2}) \Delta v \\ v_{\min}^{3, \alpha} + (i_w + \frac{1}{2}) \Delta w \end{pmatrix}. \quad (42)$$

Here we chose  $v_{\min}^{i, \alpha}$  and  $v_{\max}^{i, \alpha}$  as the cut-off in velocity boundaries as well as  $N_u^\alpha, N_v^\alpha$  and  $N_w^\alpha$  as number of quadrature points in velocity space, where we also allow to choose different discretization parameters for the different species  $\alpha$ .

**Remark 2.3** *In principle we can also choose a different, e.g. higher order or adaptive, integration rule for the current density in this case. We chose mid-point, (following the choice from our previous work on the electro-static Vlasov equation<sup>[63]</sup>) for the following benchmarks because for smooth initial conditions  $f$  is also smooth and hence the mid-point rule converges exponentially fast in theory, while being easy to implement.<sup>[68]</sup> For complicated multi-species simulations we, however, suggest using the adaptive third order scheme (with adaptive velocity boundary) presented by Wilhelm et al. on multi-species, electro-static turbulence.<sup>[4]</sup>*

Next we discretize the equations corresponding with  $\mathcal{H}_B$ :

$$f_2^\alpha(\mathbf{x}, \mathbf{v}) = f_1^\alpha(\mathbf{x}, \exp(-\frac{q^\alpha}{m_\alpha} \Delta t J_{B_1(\mathbf{x})}) \mathbf{v}), \quad (43)$$

$$\mathbf{B}_2(\mathbf{x}) = \mathbf{B}_1(\mathbf{x}), \quad (44)$$

$$\mathbf{E}_2(\mathbf{x}) = \mathbf{E}_1(\mathbf{x}) + \Delta t \nabla_{\mathbf{x}} \times \mathbf{B}_1(\mathbf{x}). \quad (45)$$

Plugging (37) – (40) into the above we obtain

$$f_2^\alpha(\mathbf{x}, \mathbf{v}) = \tilde{f}_0^\alpha \left( \mathbf{x} - \Delta t \left( \exp \left( -\frac{q^\alpha}{m_\alpha} \Delta t J_{B_0(\mathbf{x})} \right) \mathbf{v} \right), \exp \left( -\frac{q^\alpha}{m_\alpha} \Delta t J_{B_0(\mathbf{x})} \right) \mathbf{v} \right), \quad (46)$$

$$\mathbf{B}_2(\mathbf{x}) = \tilde{\mathbf{B}}_0(\mathbf{x}), \quad (47)$$

$$\mathbf{E}_2(\mathbf{x}) = \tilde{\mathbf{E}}_0(\mathbf{x}) - \hat{\mathbf{j}}(\mathbf{x}) + \Delta t \nabla_{\mathbf{x}} \times \tilde{\mathbf{B}}_0(\mathbf{x}). \quad (48)$$

Finally we can also plug this into the analytic solution corresponding to  $\mathcal{H}_E$  to obtain

$$f_3^\alpha(\mathbf{x}, \mathbf{v}) = f_2^\alpha(\mathbf{x}, \mathbf{v} - \Delta t \frac{q_\alpha}{m_\alpha} \mathbf{E}_2(\mathbf{x})), \quad (49)$$

$$\mathbf{B}_3(\mathbf{x}) = \mathbf{B}_2(\mathbf{x}) - \Delta t \nabla_{\mathbf{x}} \times \mathbf{E}_2(\mathbf{x}), \quad (50)$$

$$\mathbf{E}_3(\mathbf{x}) = \mathbf{E}_2(\mathbf{x}). \quad (51)$$

Hence for the final formula for  $f_3^\alpha$  we get

$$f_3^\alpha(\mathbf{x}, \mathbf{v}) = \tilde{f}_0^\alpha \left( \mathbf{x} - \Delta t \left( \Delta t \frac{q_\alpha}{m_\alpha} \exp(-J_{\tilde{\mathbf{B}}_0(\mathbf{x})}) (\mathbf{v} - \Delta t \frac{q_\alpha}{m_\alpha} (\tilde{\mathbf{E}}_0(\mathbf{x}) - \hat{\mathbf{j}}(\mathbf{x}) + \Delta t \nabla_{\mathbf{x}} \times \tilde{\mathbf{B}}_0(\mathbf{x}))) \right) \right), \quad (52)$$

$$\exp(J_{\tilde{\mathbf{B}}_0(\mathbf{x})} \Delta t) (\mathbf{v} - \Delta t \frac{q_\alpha}{m_\alpha} (\tilde{\mathbf{E}}_0(\mathbf{x}) - \hat{\mathbf{j}}(\mathbf{x}) + \Delta t \nabla_{\mathbf{x}} \times \tilde{\mathbf{B}}_0(\mathbf{x}))).$$

For  $\mathbf{B}_3$  we get

$$\mathbf{B}_3(\mathbf{x}) = \tilde{\mathbf{B}}_0(\mathbf{x}) - \Delta t \nabla_{\mathbf{x}} \times \tilde{\mathbf{E}}_0(\mathbf{x}) - \Delta t^2 \nabla_{\mathbf{x}} \times \hat{\mathbf{j}}(\mathbf{x}) + \Delta t^2 \nabla_{\mathbf{x}} \times \nabla_{\mathbf{x}} \times \tilde{\mathbf{B}}_0(\mathbf{x}) \quad (53)$$

and for  $\mathbf{E}_3(\mathbf{x})$  we get

$$\mathbf{E}_3(\mathbf{x}) = \tilde{\mathbf{E}}_0(\mathbf{x}) - \hat{\mathbf{j}}(\mathbf{x}) + \Delta t \nabla_{\mathbf{x}} \times \tilde{\mathbf{B}}_0(\mathbf{x}). \quad (54)$$

These formulas can now be used to construct a scheme similar to the electro-static NuFI. For this we first define the numerical flow approximation given by the advection formulas (37), (38) and (40), and denote it for the time-step  $n \in \mathbb{N}$  by

$$f^\alpha(t_n, \mathbf{x}, \mathbf{v}) = f_3^\alpha(\mathbf{x}, \mathbf{v}) = f^\alpha(\Psi_{t_n}^{t_{n+1}, \alpha}(\mathbf{x}, \mathbf{v})). \quad (55)$$

Thus if the evolution of the electromagnetic fields  $\mathbf{E}$  and  $\mathbf{B}$  as well as the (shifted) current density  $\hat{\mathbf{j}}$  is known for  $t = 0, \dots, t_n$  we can evaluate  $f^\alpha(t_{n+1})$  at an arbitrary position in phase space through

$$f^\alpha(t_{n+1}, \mathbf{x}, \mathbf{v}) = f_0^\alpha \circ \Psi_{t_0}^{t_1} \circ \dots \circ \Psi_{t_n}^{t_{n+1}}(\mathbf{x}, \mathbf{v}) = f_0^\alpha(\Psi_{t_0}^{t_{n+1}}(\mathbf{x}, \mathbf{v})). \quad (56)$$

Hence we can now formulate the full NuFI algorithm for the multi-species Vlasov–Maxwell system using the Hamiltonian splitting (NuFI-Ham).

---

**Algorithm 1** Numerical Flow Iteration for the (multi-species) Vlasov–Maxwell system (NuFI-Ham).

---

```

function NuFI( $f_0^\alpha, \mathbf{B}_0, \mathbf{E}_0, N_t, \Delta t, (N_{x_i}^\alpha)_{i,\alpha}, (N_{v_i}^\alpha)_{i,\alpha}, (v_{\min}^{i,\alpha})_{i,\alpha}, (v_{\max}^{i,\alpha})_{i,\alpha}$ )
  Interpolate  $\mathbf{E}_0$  and  $\mathbf{B}_0$  on spatial grid.
  Evaluate  $\hat{\mathbf{j}}_0$  on spatial grid with  $\tilde{f}_0 = f_0$  using (41).
  Interpolate  $\hat{\mathbf{j}}_0$  on spatial grid.
  for  $n = 1, \dots, N_t$  do
    Evaluate  $\mathbf{E}(t_n)$  on spatial grid using (54) with  $\tilde{\mathbf{E}}_0 = \mathbf{E}(t_{n-1}, \cdot)$  and interpolate.
    Evaluate  $\mathbf{E}(t_n)$  on spatial grid using (53) with  $\tilde{\mathbf{B}}_0 = \mathbf{B}(t_{n-1}, \cdot)$  and interpolate.
    Evaluate  $\hat{\mathbf{j}}(t_n)$  on spatial grid using (56) to evaluate  $f(t_n)$  as well as (41) and interpolate.
  end for
end function

```

---

## 2.4. Combing NuFI with a Predictor–Corrector Maxwell update

In section 2.3 we discussed Lie splitting with the order

$$F(t) = \exp(\mathcal{H}_E) \exp(\mathcal{H}_B) \exp(\mathcal{H}_f) F(0), \quad (57)$$

following Crouseilles et al..<sup>[66]</sup> While this choice reduces the number of operations we need to evaluate the intermediate current density  $\hat{\mathbf{j}}$ , this particular choice also introduces a restrictive Courant–Friedrichs–Lowy (CFL) condition

$$\Delta t \lesssim \min \left( \min_{i=1,2,3} (\Delta x_i, \Delta v_i) \right) \quad (58)$$

depending not only on  $\Delta \mathbf{x}$  but also  $\Delta \mathbf{v}$ . This is due to the explicit Maxwell advection relying on the interaction of  $\Delta t$  and  $\Delta \mathbf{v}$  in the integration to obtain the intermediate current density  $\hat{\mathbf{j}}$ . In practice, if the thermal velocity becomes small, this forces us to take much smaller time steps than our spatial domain size and resolution would force us to, i.e., slow the simulation unnecessarily down. However, if we change the order of the operators to

$$F(t) = \exp(\mathcal{H}_f) \exp(\mathcal{H}_B) \exp(\mathcal{H}_E) F(0) \quad (59)$$

the problematic integral can be avoided by using a separate Maxwell solver to advance the electro-magnetic fields and only using the operator splitting for the evaluation of  $f$ .

Follow the same recipe as above, but using the changed operator order 59, we get by applying  $\mathcal{H}_E$  to  $F(0) = (f_0, \mathbf{E}_0, \mathbf{B}_0)$

$$f_1(\mathbf{x}, \mathbf{v}) = f_0(\mathbf{x}, \mathbf{v} - \Delta \frac{q_\alpha}{m_\alpha} \mathbf{E}_0(\mathbf{x})). \quad (60)$$

After applying  $\mathcal{H}_B$  we get

$$f_2(\mathbf{x}, \mathbf{v}) = f_1(\mathbf{x}, \exp(-\frac{q_\alpha}{m_\alpha} \Delta t J_{\mathbf{B}_1(\mathbf{x})}) \mathbf{v} - \Delta t \frac{q_\alpha}{m_\alpha} \mathbf{E}_0(\mathbf{x})). \quad (61)$$

We have

$$\mathbf{B}_1(\mathbf{x}) = \mathbf{B}_0 - \Delta t \nabla_{\mathbf{x}} \times \mathbf{E}_0(\mathbf{x}) \quad (62)$$

and for simplicity of notation we denote

$$\mathbf{v}_2(\mathbf{x}) = \exp(-\frac{q_\alpha}{m_\alpha} \Delta t J_{\mathbf{B}_0 - \Delta t \nabla_{\mathbf{x}} \times \mathbf{E}_0(\mathbf{x})}) \mathbf{v} - \Delta t \frac{q_\alpha}{m_\alpha} \mathbf{E}_0(\mathbf{x}). \quad (63)$$

Finally, we can apply  $\mathcal{H}_f$

$$f_3(\mathbf{x}, \mathbf{v}) = f_2(\mathbf{x} - \Delta t \mathbf{v}, v) \quad (64)$$

and hence the NuFI-update formula becomes

$$f(t_{n+1}, \mathbf{x}, \mathbf{v}) = f(t_n, \tilde{\mathbf{x}}, \mathbf{v}_2(\tilde{\mathbf{x}})), \quad (65)$$

where we denote  $\tilde{\mathbf{x}} = \mathbf{x} - \Delta \mathbf{v}$ .

The new NuFI-update formula does not depend on intermediate evaluations of the current density, which means that we can now predict  $\rho^{n+1}$  as well as  $\mathbf{j}^{n+1}$  without knowledge of the electro-magnetic fields at  $t^{n+1}$  and thus can use a that information for a more robust Maxwell solver. For our implementation we chose the predictor-corrector approach.<sup>[39]</sup> Discretizing  $\mathbf{E}$  and  $\mathbf{B}$  on a uniform in space but staggered in time grid we use

$$\mathbf{E}^{n+1} = \mathbf{E}^n + \Delta t \nabla_{\mathbf{x}} \times \mathbf{B}^{n+1/2} - \frac{\Delta t}{2} (\mathbf{j}^n + \mathbf{j}^{n+1}), \quad (66)$$

$$\mathbf{B}^{n+1/2} = \mathbf{B}_{n-1/2} - \Delta t \nabla_{\mathbf{x}} \times \mathbf{E}^n. \quad (67)$$

The thus obtained values are then interpolated on the spatial grid using B-Splines. Because we require  $\mathbf{B}^n$  for (65), we also compute and interpolate

$$\mathbf{B}^n = \frac{1}{2} (\mathbf{B}^{n+1/2} + \mathbf{B}^{n-1/2}). \quad (68)$$

Furthermore, if we only prescribe  $\mathbf{B}_0$  then  $\mathbf{B}_{-1/2}$  can be predicted via

$$\mathbf{B}^{-1/2} = \mathbf{B}_0 + \frac{\Delta t}{2} \nabla_{\mathbf{x}} \times \mathbf{E}_0. \quad (69)$$

As we now no longer depend on an intermediate current density the CFL condition reduces back to

$$\Delta t \lesssim \min_{i=1,2,3} \Delta x_i. \quad (70)$$

Additionally, in this version we no longer have to store the evolution of the intermediate current density, which reduces the memory footprint of the scheme, and as we no longer take second derivatives in the field solver we are now also free to choose one order lower interpolation B-Splines while retaining the same spatial accuracy.

This leaves us with the following NuFI-PC algorithm

---

**Algorithm 2** Numerical Flow Iteration for the (multi-species) Vlasov–Maxwell system coupled with Predictor–Corrector. (NuFI-PC)

---

```

function NuFI( $f_0^\alpha$ ,  $\mathbf{B}_0$ ,  $\mathbf{E}_0$ ,  $N_t$ ,  $\Delta t$ ,  $(N_{x_i}^\alpha)_{i,\alpha}$ ,  $(N_{v_i}^\alpha)_{i,\alpha}$ ,  $(v_{\min}^{i,\alpha})_{i,\alpha}$ ,  $(v_{\max}^{i,\alpha})_{i,\alpha}$  )
  Interpolate  $\mathbf{E}_0$  and  $\mathbf{B}_0$  on spatial grid.
  Compute and interpolate  $\mathbf{B}_{-1/2}$  via (69).
  Compute  $\mathbf{j}_0$  on spatial grid using (65) and a midpoint rule.
  Compute and interpolate  $\mathbf{B}_{1/2}$  using (67).
  for  $n = 1, \dots, N_t$  do
    Compute  $\mathbf{j}_n$  on spatial grid using (65) and a midpoint rule.
    Compute and interpolate  $\mathbf{E}^n$  using (66).
    Compute and interpolate  $\mathbf{B}_{n+1/2}$  using (67).
    Compute and interpolate  $\mathbf{B}^n$  using (68).
     $\mathbf{j}_{n-1} = \mathbf{j}_n$ .
  end for
end function

```

---

## 2.5. Reducing the Computational Complexity of NuFI

As discussed in section 2.1, NuFI has a computational complexity of  $\mathcal{O}(n_t^2)$  both in the electrostatic as well as now in the electro-magnetic case. As we explicitly discretize the Maxwell’s equations in the fully electro-magnetic case, we also introduce a CFL-type stability restriction on our approach, which restricts the choice of time-step size and requires us to make more steps. Hence the simulation of long time periods would become prohibitively expensive with the pure NuFI. The authors have discussed approaches to remedy this in previous publications, which we will quickly recap in this section.<sup>[4],[69]</sup>

The quadratic computational complexity can be reduced back to linear by restarting NuFI through storing a snapshot of the distribution functions for each species each  $n_t^r > 0$  time-steps and replacing  $f_0^\alpha$  by the stored snapshot. This is similar to a Semi-Lagrangian approach with sub-cycling for all species, however, without the need to store the intermediate results, and in fact if we let  $n_t^r \rightarrow 1$ , then this approach becomes equivalent to a classic backwards Semi-Lagrangian scheme.

In the prototype implementation used in this work we employ linear interpolation on a uniform grid to store the snapshots. While quite simplistic, it is sufficient to resolve the low-dimensional test cases, which we are interested in as a proof-of-concept in section 3. Furthermore, this storage option is naturally compatible with low rank compression.<sup>[69],[70]</sup>

**Remark 2.4** *The major draw-back of linear interpolation is its dissipative nature, which becomes problematic for frequent restarts or very long simulations. While the thus introduced numerical dissipation is still significantly less pronounced than for a comparable Semi-Lagrangian simulation, the associated errors build up for long simulations and therefore are no longer negligible.*

*Improved restart procedures are under investigation in on-going work. In particular, a promising alternative is – instead of storing the distribution function – to store the flow map directly following the Characteristic Mapping Method (CMM) approach.<sup>[62]</sup> This approach has been recently explored for the electro-static case and is promising due to its additional structure-preservation properties in comparison to direct discretization of the distribution function.<sup>[71]</sup>*

### 3. Numerical Tests

In the following we are testing algorithms 1 and 2 for a number of classical benchmarks. First we look at *weak Landau damping* to test the consistency of the Vlasov–Maxwell solver in the electro-static limit. Then we look at a *streaming Weibel instability* as well as the *filamentation instability* test cases in  $1x2v$ .

The implementation used for the simulations can be found in the NuFI GitHub repository<sup>4</sup> in the branch *tensor\_svd\_approx*. The implementation is natively in six-dimensions and allows for electrons as well as ions of arbitrary mass and charge. However, we decided to only show results of simulations in the dimension-reduced settings to keep the focus of this paper on a proof-of-concept of the novel algorithm. Higher dimensional simulations are part of on-going work.

Note that the parameter space, such as frequency and grid resolution, for restarts has been explored in previous work and identified good parameter choices. The parameter choices made for the following simulations are therefore based upon these previous studies.<sup>[4],[69]</sup>

#### 3.1. Weak Landau Damping

Before we move on to fully electro-magnetic simulations, we check whether the new algorithms also converge back to the solution of the Vlasov–Poisson system if going towards the electro-static limit. To this end we chose the classic *weak Landau damping* benchmark. For the initial data we have

$$f_0(x, v) = \frac{1}{\sqrt{2\pi}}(1 + \alpha \cos(kx)) \exp(-\frac{v^2}{2}), \quad (71)$$

where  $\alpha = 0.01$  and  $k = 0.5$ . The initial electric field is

$$\mathbf{E}_0(x) = \begin{pmatrix} -\frac{\alpha}{k} \sin(kx) \\ 0 \\ 0 \end{pmatrix} \quad (72)$$

and  $\mathbf{B}_0 = 0$ . The  $y$  and  $z$  direction are set to be uniform and for the  $x - v_x$  phase-space we choose  $[0, \frac{2\pi}{k}] \times [-5, 5]$ . As base resolution for both NuFI-Ham and NuFI-PC we choose  $N_x = 32$  and  $N_v = 32$ .

In figure 1 we show the evolution of the electric energy over time. The expected damping rate  $\gamma = -0.15336$  of the electric field is recovered exactly by NuFI-Ham even with a time-step as large as  $\frac{1}{5}$ , however, NuFI-PC is less accurate with the large time step and exhibits some minor energy overshoots after  $t \approx 15$ , but recovers after the recurrence. Decreasing  $\Delta t$  also decreases the strength of the overshoots, which suggests that even though both NuFI-Ham and NuFI-PC are technically first order in time the field solver coming from the Hamiltonian splitting is more accurate than the predictor-corrector scheme employed for NuFI-PC.

Both NuFI-Ham and NuFI-PC are consistent with the electro-static limit and, in fact,  $\mathbf{B} = 0$  is preserved throughout the entire simulation.

#### 3.2. Streaming Weibel Instability

The Streaming Weibel Instability is a classic kinetic instability used to test electro-magnetic solvers for the Vlasov system. Here we consider the setup suggested by Cheng et al. and Kormann et al..<sup>[16],[72]</sup> The  $y$  and  $z$  spatial components as well as  $v_z$  velocity directions are assumed to be

<sup>4</sup><https://github.com/paulwilhelmvlasov/NumericalFlowIteration>

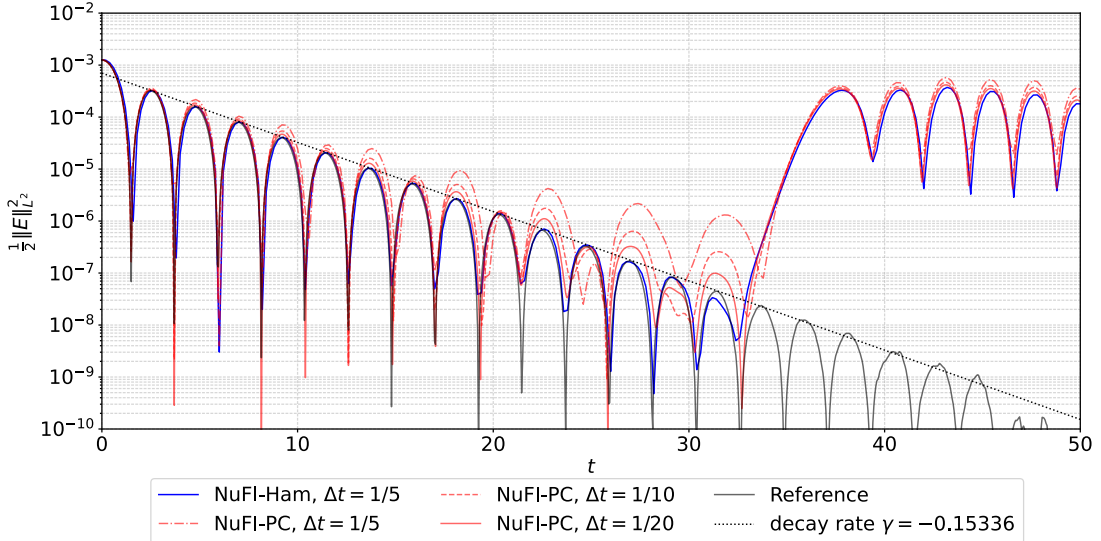


Figure 1: Comparison between NuFI-Ham, NuFI-PC and a reference solution (electro-static NuFI) of the *Weak Landau Damping* benchmark. The analytically predicted decay rate is  $\gamma = -0.15336$ , which is captured by all approaches, however, less precisely by NuFI-PC than NuFI-Ham.

uniform and therefore the system reduces to  $1x2v$ . Additionally we can assume an uniform ion distribution<sup>5</sup> and a periodic boundary in the  $x$ -direction. The initial electron distribution has a temperature anisotropy as  $T_y > T_x$ :

$$f_0(x, u, v) = \frac{1}{2\pi\sigma} \exp\left(-\frac{u^2}{2\sigma^2}\right) \left( \delta \exp\left(\frac{(v-v_1)^2}{2\sigma^2}\right) + (1-\delta) \exp\left(\frac{(v-v_2)^2}{2\sigma^2}\right) \right), \quad (73)$$

where  $x \in [0, \frac{2\pi}{\theta}]$  and  $\theta = 0.2$ . The initial electric field is 0 and the initial magnetic field is set to

$$\mathbf{B}_0(x) = \begin{pmatrix} 0 \\ 0 \\ \beta \sin(\theta x) \end{pmatrix}. \quad (74)$$

We truncate the velocity domain to  $[-0.5, 0.5] \times [-1.2, 1.2]$ . The phase-space resolution used is  $32 \times 32 \times 32$ . For NuFI-Ham we used  $\Delta t = \frac{1}{200}$  as larger time-steps were not possible due to the CFL-condition (58). For NuFI-PC larger time-steps were possible so we consider  $\Delta t = \frac{1}{10}, \frac{1}{50}$  and  $\Delta t = \frac{1}{100}$ . The restart time for both approaches was set to  $n_t^r = 100$ .

**Remark 3.1** Note that Kormann *et al.* report a CFL condition

$$\Delta t = \lambda \frac{\min(\min_{i=1,2,3}(\Delta x_i, \Delta v_i))}{k\beta}, \quad (75)$$

with  $\beta = \|(\mathbf{v}, \mathbf{E} + \mathbf{v} \times \mathbf{B})\|_{L^\infty}$  and the chosen CFL number 0.4, making it comparable to the one for NuFI-Ham. Hence while they do not explicitly state their used time step it is comparable to what we used for NuFI-Ham.

<sup>5</sup>For ease of readability we drop the  $e$  index in this section.

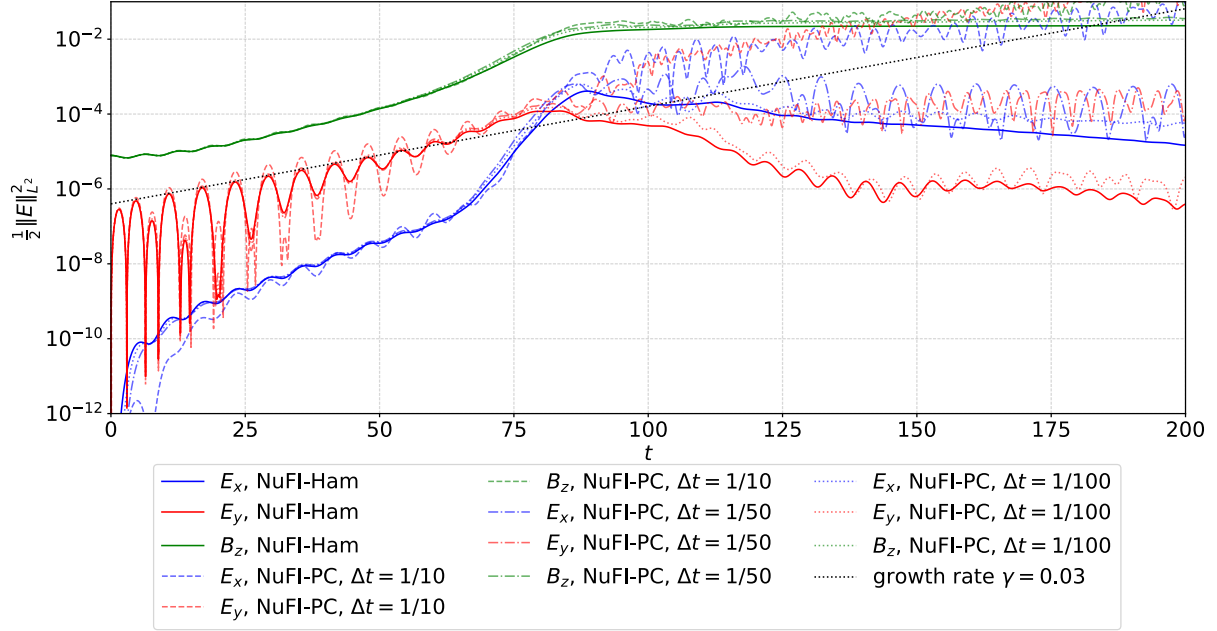


Figure 2: Evolution of the energies associated to the components of the electric and magnetic fields over time for the *streaming Weibel instability* compared between NuFI-Ham and NuFI-PC. The analytically predicted growth rate  $\gamma = 0.03$  of the electric energy is well matched with the simulation results.

In figure 2 we show the energies associated to the components of the electric and magnetic energies. The linear growth with growth rate  $\gamma = 0.03$  of the  $E_y$  component is well reproduced by the NuFI simulation. The dynamics produced by both approaches are overall in good agreement with the reference simulation from Kormann et al.<sup>[16]</sup> until  $t \approx 80$ , even though we used only half as many degrees of freedom in velocity space. The analytically predicted growth rate of  $\gamma = 0.03$  of the  $y$ -component of the electric field is well captured by both NuFI-PC and NuFI-Ham.

Similar to the *weak Landau damping* case, see section 3.1, we see that the error in time for NuFI-PC dominates and hence with large time steps the electric field oscillates more than expected. After  $t \approx 80$  NuFI-Ham and NuFI-PC start deviating substantially. While NuFI-PC with  $\Delta t = \frac{1}{10}$  does not blow up and was able to reproduce the onset of the instability, the electric energy error grows quickly in the non-linear stage. With decreasing  $\Delta t$  the NuFI-PC solution converges towards the NuFI-Ham solution. This suggests that while NuFI-PC technically avoids the restrictive CFL condition of NuFI-Ham, for high fidelity one would either have still go to small time-steps – comparable to NuFI-Ham – or directly use NuFI-Ham. Finally, when comparing the late stage of the simulation with the results of Kormann et al., we observe that their FEM solution also exhibits fast, unphysical oscillations similar to NuFI-PC.

Next we also looked at the distribution functions produced by NuFI-Ham. Note that the distribution function errors between NuFI-Ham and NuFI-PC were negligible, we only show  $f$  from NuFI-Ham as representative for both approaches. In figure 4 we show cross-sections of the distribution function in at  $u = 0$  and  $v = 0$  respectively for time  $t = 50, 100$  and  $200$ . Furthermore, in figure 5, we also show the distribution function at the left boundary as well as in the middle of the spatial domain. The displayed distribution functions are in good agreement reference solution in Cheng et al.<sup>[72]</sup> Even with the low phase-space resolution used for this simulation – combined with linear interpolation for restarts – we still retain good sub-grid resolution, also called the

*zoom property*, which is characteristic to kinetic solvers directly discretizing the flow map like NuFI or CMM.<sup>[62]</sup> The zoom property was previously only observed for the electro-static case and retaining it is a good indicator that the extension using the Hamiltonian splitting allows to preserve the solution structure to a similar degree as in the (simpler) electro-static case. To showcase this we also zoomed deeper into the low density region of the velocity space around the left spatial domain boundary, see figure 6. Even when zooming below the grid resolution, we still obtain a noise-free and finely resolved distribution function.

Finally, in figure 3 we also look at the conservation properties of NuFI-Ham and NuFI-PC. Note that for this simulation we refrained from using restarts as these are well-known to break the conservation properties<sup>[69]</sup> and we are only interested in whether the conservation properties of the electro-static NuFI<sup>[63]</sup> carry over to the fully electro-magnetic setting. The simulations were performed with a phase-space resolution of  $16^3$  for both approaches, while the time step was chosen as  $\Delta t = \frac{1}{200}$  for NuFI-Ham and  $\Delta t = \frac{1}{10}$  for NuFI-PC. The kinetic energy and entropy are both computed using a midpoint rule as we do not have the distribution function on a grid of  $64^3$ . The measured relative errors of NuFI-PC exceed those of NuFI-Ham, however, all measured errors are less than the numerical quadrature error. The entropy is exactly preserved by NuFI-Ham until  $t \approx 45$  after which the measured error remains below  $10^{-5}$ . The relative total energy error of NuFI-Ham remains constantly below  $10^{-3}$  for all times. NuFI-PC shows a steady increase in both relative errors over time, which leads us to the conclusion that the Maxwell solver through the predictor-corrector scheme breaks the otherwise preserved conservation properties obtained by the Hamiltonian splitting.

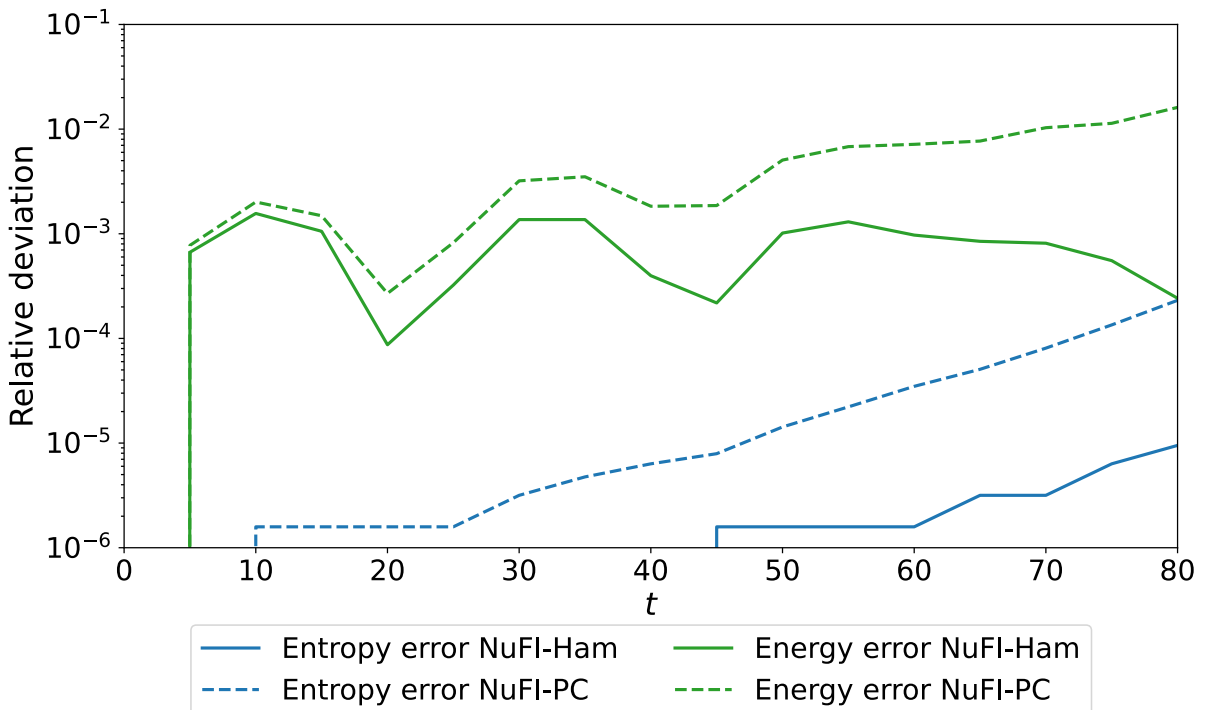


Figure 3: Conservation of total energy and entropy over time for the *streaming Weibel instability* in simulation of NuFI-PC and NuFI-Ham with  $16^3$  and  $\Delta t = \frac{1}{10}$ .

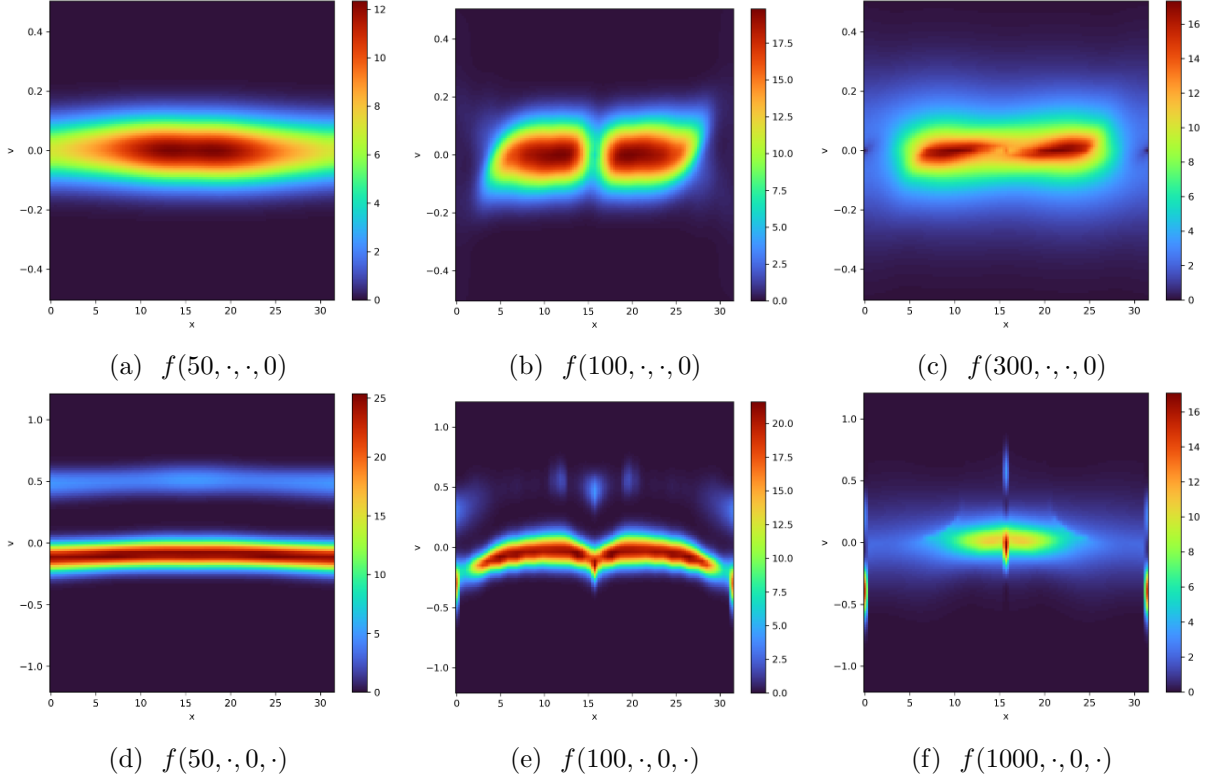


Figure 4: Cross-sections of the velocity distribution function  $f$  for the *streaming Weibel instability* at  $u = 0$  (top) and at  $v = 0$  (bottom) at times  $t = 50, 100$  and  $300$  (from left to right).

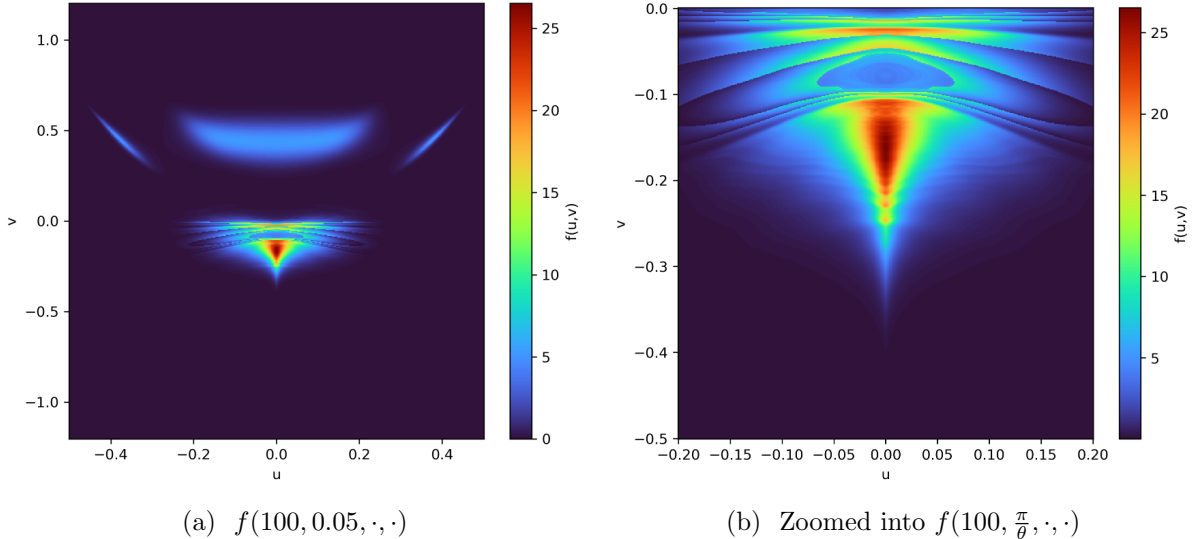


Figure 5: Velocity distribution function  $f$  for the *streaming Weibel instability* close to the left boundary ( $x = 0.05$ , left figure) and in the middle of the spatial domain (right figure) at the time  $t = 100$ .

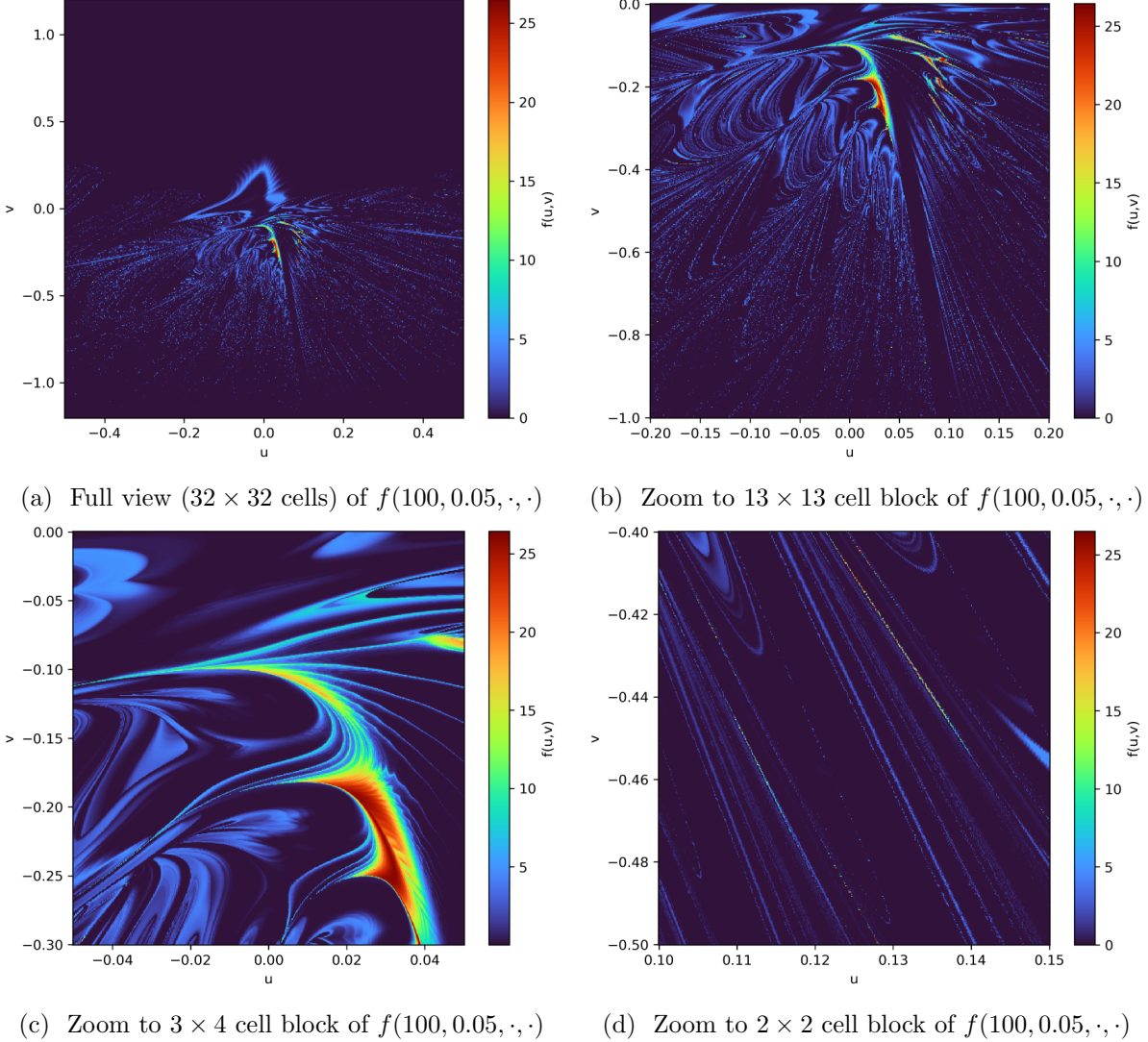


Figure 6: In this figure we look into the velocity distribution function  $f$  for the *streaming Weibel instability* at  $x = 0.05$  and time  $t = 100$  while zooming increasingly in. The method is able to clearly resolve sub-grid structures far beyond the common capability of the linear interpolation technique used for the restarts or that of state-of-the-art Semi-Lagrangian solvers.

### 3.3. Filamentation Instability

Next we consider the *filamentation instability*, a fully electro-magnetic variant of the (electrostatic) *two stream instability*. The initial condition are two beams in  $v_y$  direction, i. e., perpendicular to the dominant spatial direction:

$$f_0(x, u, v) = \frac{1}{2} \exp\left(-\frac{v^2}{2v_{\text{th}}^2}\right) \left( \exp\left(-\frac{(u-v_b)^2}{2v_{\text{th}}^2}\right) + \exp\left(-\frac{(u+v_b)^2}{2v_{\text{th}}^2}\right) \right), \quad (76)$$

where the thermal velocity is uniformly set to  $v_{\text{th}} = 0.1$  and the beam velocity to  $v_b = 0.4$ .

The instability is triggered through an initial magnetic field

$$\mathbf{B}_0(x) = \begin{pmatrix} 0 \\ 0 \\ \beta \cos(kx) \end{pmatrix}, \quad (77)$$

with perturbation strength  $\beta = 10^{-3}$  and mode  $k = 2$ . The spatial domain is  $[0, \frac{2\pi}{k}]$  and the velocity domain is truncated to  $[-1, 1] \times [-1.2, 1.2]$ . We use NuFI-PC for our simulations with  $32^3$  and  $64^3$  as well as  $\Delta t = \frac{1}{20}$  and  $= \frac{1}{50}$  as time step.

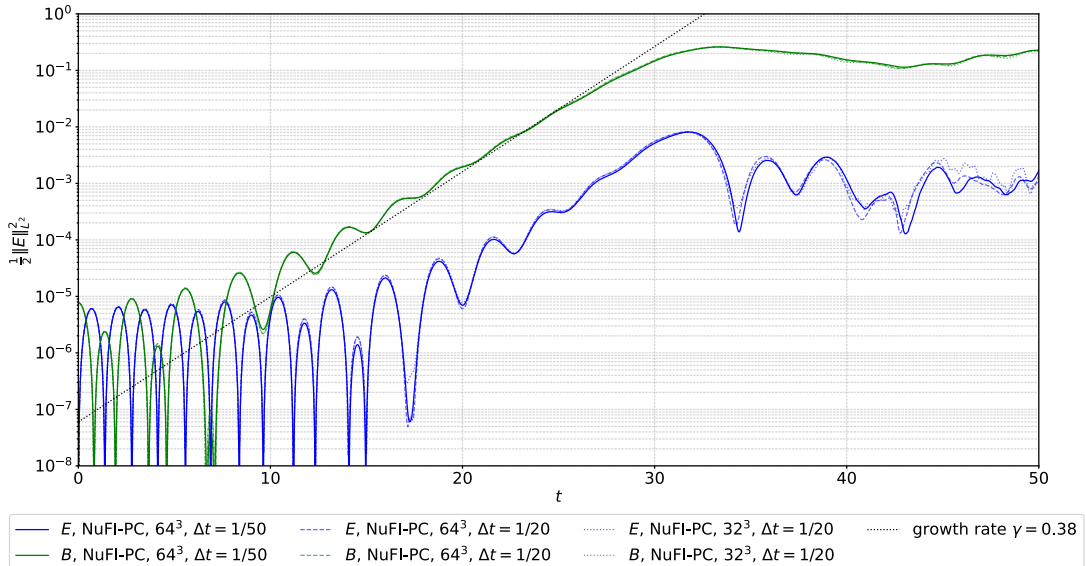


Figure 7: Evolution of electric and magnetic energy over time for a simulation of the *Filamentation instability* performed by NuFI-PC.

We expect a growth rate of roughly  $\gamma \approx 0.38$  for the magnetic field energy, see appendix B. Taking the finite wavenumber  $k$  and the finite transverse thermal spread of the beams into account, the growth rate is captured well by our simulation, see figure 7. The magnetic energy is practically indistinguishable between the different resolutions, whereas the simulations with smaller time steps show small deviations after  $t \approx 30$  in the electric field energy.

In figure 8 we look at cross-sections of the distribution function at  $t = 50$ . Similar to what we already saw with NuFI-Ham in the previous section, here with NuFI-PC the distribution function is also well-resolved and noise-free. The filamentation can be particularly well observed in figure 8b.

## 4. Discussion and outlook

In this work we presented two ways, NuFI-Ham and NuFI-PC, to extend the electro-static NuFI algorithm to the fully electro-magnetic setting by employing the Hamiltonian structure of the Vlasov–Maxwell system. We have shown that strong structure-preserving properties of NuFI are preserved when going from the electro-static to the electro-magnetic system, making NuFI also an interesting high-fidelity but low-memory cost approach for kinetic plasma dynamics in the electro-magnetic case. Through restarting the simulation periodically in time we also were

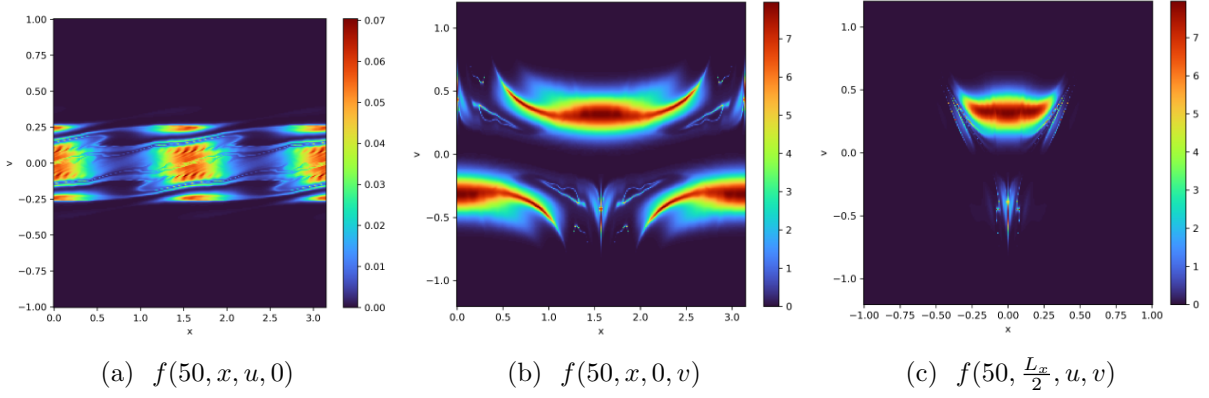


Figure 8: Cross-section of distribution functions from the simulation of the *filamentation instability* with NuFI-PC using a resolution of  $64^3$  in phase-space and  $\Delta t = \frac{1}{50}$ .

able to reduce the computational complexity sufficiently such that long simulations were enabled, while retaining most of the structure-preservation in NuFI.

In on-going and future work we want to look into simulations of fully six-dimensional kinetic plasma dynamics, e.g. of beam-driven instabilities.<sup>[73],[74]</sup> While the code is already written in such a way that six-dimensional simulations, including multi-species, are already possible, simulations of very long time-scales as they are common in e.g. astrophysical settings suffer noticeably from the dissipative nature of our restart routine currently based upon linear interpolation. Hence we currently also investigate advanced restarting routines to improve both performance and structure-preservation.

## Acknowledgments

R.-P.W. wants to thank the organizers of the National High Performance Computing (NHR) graduate school and the Federal Ministry of Education and Research as well as the state governments for supporting this work as part of the joint funding of National High Performance Computing (NHR). R.-P.W. wants to thank the DFG, who funded part of the work through the IRTG Modern Inverse Problems (333849990/GRK2379). This work has received funding from the European High Performance Computing Joint Undertaking (JU) and Belgium, Czech Republic, France, Germany, Greece, Italy, Norway, and Spain under grant agreement No 101093441. Views and opinions expressed are however those of the author(s) only and do not necessarily reflect those of the European Union or the European High Performance Computing Joint Undertaking (JU) and Belgium, Czech Republic, France, Germany, Greece, Italy, Norway, and Spain. Neither the European Union nor the granting authority can be held responsible for them. F.B. acknowledges support from the FED-tWIN programme (profile Prf-2020-004, project “ENERGY”) issued by BELSPO, and from the FWO Junior Research Project G020224N granted by the Research Foundation – Flanders (FWO). The resources and services used in this work were provided by the VSC (Flemish Supercomputer Center), funded by the Research Foundation - Flanders (FWO) and the Flemish Government.

## A. Normalization of the multi-species Vlasov–Maxwell system

We choose to normalize the Vlasov–Maxwell system to the electron scales, i.e., we choose as reference the electron charge  $q_e = e$ , electron mass  $m_e$  and the electron number density  $n_0$ . The electron plasma frequency is

$$\omega_{p,e}^2 = \frac{4\pi n_0 e^2}{m_e}. \quad (78)$$

Hence we choose as a reference scale for time  $t_0 = \omega_{p,e}^{-1}$ , spatial dimension  $L_0 = \frac{c}{\omega_{p,e}}$  and velocity  $V_0 = c$ . Consequentially we choose for the fields  $E_0 = \frac{m_e c \omega_{p,e}}{e}$ ,  $B_0 = E_0$ ,  $f_0 = \frac{n_0}{V_0^3} = \frac{n_0}{c^3}$ . Finally the charge and current density are scaled to  $\rho_0 = e n_0$  and  $J_0 = e c n_0$  respectively.

Then our dimensionless variables used in (1) – (7) are

$$\begin{aligned} t' &= \frac{t}{t_0}, & x' &= \frac{x}{L_0}, & v' &= \frac{v}{V_0}, \\ f'_s &= \frac{f_s}{f_0}, & E' &= \frac{E}{E_0}, & B' &= \frac{B}{B_0}, \\ \rho' &= \frac{\rho}{\rho_0}, & J' &= \frac{J}{J_0}. \end{aligned} \quad (79)$$

For the sake of readability we dropped the primes.

## B. Growth rate of filamentation instability

For two symmetric, cold counter-streaming electron beams with drift speeds  $\pm v_b$  and total plasma frequency  $\omega_{pe}$ , the transverse filamentation instability has the cold-limit growth rate

$$\gamma_{\text{cold}} = \frac{\beta_b}{\sqrt{\gamma_0}} \omega_{pe}, \quad \beta_b = \frac{v_b}{c}, \quad \gamma_0 = (1 - \beta_b^2)^{-1/2}, \quad (80)$$

see, e.g., Bret et al.<sup>[75]</sup> For the parameters used here,  $v_b = 0.4$  and  $\omega_{pe} = 1$ , we have  $\gamma_0 \approx 1.091$  and therefore the expected linear growth rate is

$$\gamma_{\text{cold}} = \frac{0.4}{\sqrt{1.091}} \approx 0.38. \quad (81)$$

## References

- [1] F. Chen. *Introduction to Plasma Physics and Controlled Fusion*. Springer Cham, 2015. ISBN: 978-3-319-22309-4. DOI: 10.1007/978-3-319-22309-4.
- [2] P. J. Morrison. “The Maxwell-Vlasov equations as a continuous hamiltonian system”. In: *Physics Letters A* 80.5 (1980), pp. 383–386. ISSN: 0375-9601. DOI: 10.1016/0375-9601(80)90776-8.
- [3] D. Verscharen, K. Klein and B. Maruca. “The multi-scale nature of the solar wind”. In: *Living reviews in solar physics* 16.1 (2019). DOI: 10.1007/s41116-019-0021-0.
- [4] R.-P. Wilhelm and M. Torrilhon. “Simulation of multi-species kinetic instabilities with the Numerical Flow Iteration”. In: *Accepted for publication in Proceedings of the 33rd International Symposium on Rarefied Gas Dynamics* (2025).
- [5] D. Verscharen et al. “A Case for Electron-Astrophysics”. In: *Experimental Astronomy* 54.2 (2022). DOI: 10.1007/s10686-021-09761-5.

[6] G. Lapenta et al. “Do We Need to Consider Electrons’ Kinetic Effects to Properly Model a Planetary Magnetosphere: The Case of Mercury”. In: *Journal of Geophysical Research: Space Physics* 127.4 (2022). e2021JA030241 2021JA030241, e2021JA030241. doi: 10.1029/2021JA030241.

[7] T. Arber and R. Vann. “A Critical Comparison of Eulerian-Grid-Based Vlasov Solvers”. In: *Journal of Computational Physics* 180.1 (2002), pp. 339–357. ISSN: 0021-9991. doi: 10.1006/jcph.2002.7098.

[8] F. Jenko et al. “Electron temperature gradient driven turbulence”. In: *Physics of Plasmas* 7.5 (May 2000), pp. 1904–1910. ISSN: 1070-664X. doi: 10.1063/1.874014.

[9] T. Görler et al. “The global version of the gyrokinetic turbulence code GENE”. In: *Journal of Computational Physics* 230.18 (2011), pp. 7053–7071. ISSN: 0021-9991. doi: <https://doi.org/10.1016/j.jcp.2011.05.034>.

[10] J. Juno et al. “Discontinuous Galerkin algorithms for fully kinetic plasmas”. In: *Journal of Computational Physics* 353 (2018), pp. 110–147. ISSN: 0021-9991. doi: 10.1016/j.jcp.2017.10.009.

[11] N. R. Mandell et al. “Electromagnetic full- $f$  gyrokinetics in the tokamak edge with discontinuous Galerkin methods”. In: *Journal of Plasma Physics* 86.1 (2020), p. 905860109. doi: 10.1017/S0022377820000070.

[12] E. Fijalkow. “A numerical solution to the Vlasov equation”. In: *Computer Physics Communications* 116.2 (Feb. 1999), pp. 319–328. ISSN: 0010-4655. doi: 10.1016/S0010-4655(98)00146-5.

[13] F. Filbet, E. Sonnendrücker and P. Bertrand. “Conservative Numerical Schemes for the Vlasov Equation”. In: *Journal of Computational Physics* 172.1 (Sept. 2001), pp. 166–187. ISSN: 0021-9991. doi: 10.1006/jcph.2001.6818.

[14] J. Wen and M. Nazarov. “An anisotropic nonlinear stabilization for finite element approximation of Vlasov–Poisson equations”. In: *Journal of Computational Physics* 536 (2025), p. 114079. ISSN: 0021-9991. doi: 10.1016/j.jcp.2025.114079.

[15] Y. Kiechle, E. Chudzik and C. Helzel. “A positivity-preserving Active Flux method for the Vlasov–Poisson system”. In: *Journal of Computational Physics* 524 (2025), p. 113693. ISSN: 0021-9991. doi: 10.1016/j.jcp.2024.113693.

[16] K. Kormann, M. Nazarov and J. Wen. “A structure-preserving finite element framework for the Vlasov–Maxwell system”. In: *Computer Methods in Applied Mechanics and Engineering* 446 (2025), p. 118290. ISSN: 0045-7825. doi: 10.1016/j.cma.2025.118290.

[17] C. Cheng and G. Knorr. “The integration of the Vlasov equation in configuration space”. In: *Journal of Computational Physics* 22.3 (Nov. 1976), pp. 330–351. ISSN: 0021-9991. doi: 10.1016/0021-9991(76)90053-X.

[18] L. P. Riishøjgaard et al. “The Use of Spline Interpolation in Semi-Lagrangian Transport Models”. In: *Monthly Weather Review* 126.7 (1998), pp. 2008–2016. doi: 10.1175/1520-0493(1998)126<2008:TUOSII>2.0.CO;2.

[19] K. Kormann, K. Reuter and M. Rampp. “A massively parallel semi-Lagrangian solver for the six-dimensional Vlasov–Poisson equation”. In: *The International Journal of High Performance Computing Applications* 33.5 (2019), pp. 924–947. doi: 10.1177/1094342019834644.

[20] L. Einkemmer. “High performance computing aspects of a dimension independent semi-Lagrangian discontinuous Galerkin code”. In: *Comput. Phys. Commun.* 202 (2016), pp. 326–336.

[21] N. Crouseilles, M. Mehrenberger and E. Sonnendrücker. “Conservative semi-Lagrangian schemes for Vlasov equations”. In: *Journal of Computational Physics* 229.6 (2010), pp. 1927–1953. ISSN: 0021-9991. doi: 10.1016/j.jcp.2009.11.007.

[22] G.-H. Cottet et al. “High order semi-Lagrangian particle methods for transport equations: numerical analysis and implementation issues”. In: *ESAIM: Mathematical Modelling and Numerical Analysis* 48.4 (2014), 1029–1060. doi: 10.1051/m2an/2014009.

[23] G.-H. Cottet. “Semi-Lagrangian particle methods for high-dimensional Vlasov–Poisson systems”. In: *Journal of Computational Physics* 365 (2018), pp. 362–375. ISSN: 0021-9991. doi: 10.1016/j.jcp.2018.03.042.

[24] J. A. Rossmanith and D. C. Seal. “A positivity-preserving high-order semi-Lagrangian discontinuous Galerkin scheme for the Vlasov–Poisson equations”. In: *Journal of Computational Physics* 230.16 (2011), pp. 6203–6232. ISSN: 0021-9991. doi: <https://doi.org/10.1016/j.jcp.2011.04.018>.

[25] U. Ganse et al. “The Vlasiator 5.2 ionosphere – coupling a magnetospheric hybrid-Vlasov simulation with a height-integrated ionosphere model”. In: *Geoscientific Model Development* 18.2 (2025), pp. 511–527. doi: 10.5194/gmd-18-511-2025.

[26] S. von Alfthan et al. “Vlasiator: First global hybrid-Vlasov simulations of Earth’s foreshock and magnetosheath”. In: *Journal of Atmospheric and Solar-Terrestrial Physics* 120 (2014), pp. 24–35. ISSN: 1364-6826. DOI: <https://doi.org/10.1016/j.jastp.2014.08.012>.

[27] H. Schmitz and R. Grauer. “Kinetic Vlasov simulations of collisionless magnetic reconnection”. In: *Physics of Plasmas* 13.9 (Sept. 2006), p. 092309. ISSN: 1070-664X. DOI: 10.1063/1.2347101.

[28] F. Allmann-Rahn et al. “The muphyII code: Multiphysics plasma simulation on large HPC systems”. In: *Computer Physics Communications* 296 (2024), p. 109064. ISSN: 0010-4655. DOI: 10.1016/j.cpc.2023.109064.

[29] L. Einkemmer. “A performance comparison of semi-Lagrangian discontinuous Galerkin and spline based Vlasov solvers in four dimensions”. In: *Journal of Computational Physics* 376 (2019), pp. 937–951. ISSN: 0021-9991. DOI: 10.1016/j.jcp.2018.10.012.

[30] L. Einkemmer and A. Moriggl. “Semi-Lagrangian 4d, 5d, and 6d kinetic plasma simulation on large-scale GPU-equipped supercomputers”. In: *The International Journal of High Performance Computing Applications* 37.2 (2023), pp. 180–196. DOI: 10.1177/10943420221137599.

[31] N. Schild et al. “A performance portable implementation of the semi-Lagrangian algorithm in six dimensions”. In: *Comput. Phys. Commun.* 295 (2024), p. 108973. DOI: <https://doi.org/10.1016/j.cpc.2023.108973>.

[32] K. Kormann and E. Sonnendrücker. “Sparse Grids for the Vlasov–Poisson Equation”. In: *Sparse Grids and Applications - Stuttgart 2014*. Ed. by J. Garcke and D. Pflüger. Cham: Springer International Publishing, 2016, pp. 163–190. ISBN: 978-3-319-28262-6.

[33] W. Guo and Y. Cheng. “A Sparse Grid Discontinuous Galerkin Method for High-Dimensional Transport Equations and Its Application to Kinetic Simulations”. In: *SIAM Journal on Scientific Computing* 38.6 (2016), A3381–A3409. DOI: 10.1137/16M1060017.

[34] N. Besse and E. Sonnendrücker. “Semi-Lagrangian schemes for the Vlasov equation on an unstructured mesh of phase space”. In: *Journal of Computational Physics* 191.2 (2003-11), pp. 341–376. ISSN: 0021-9991. DOI: 10.1016/S0021-9991(03)00318-8.

[35] Y. Pfau-Kempf et al. “On the Importance of Spatial and Velocity Resolution in the Hybrid-Vlasov Modeling of Collisionless Shocks”. In: *Frontiers in Physics* Volume 6 - 2018 (2018). ISSN: 2296-424X. DOI: 10.3389/fphy.2018.00044.

[36] M. Palmroth et al. “Vlasov methods in space physics and astrophysics”. In: *Living Reviews in Computational Astrophysics* 4.1 (2018). DOI: 10.1007/s41115-018-0003-2.

[37] G.-H. Cottet and P.-A. Raviart. “Particle Methods for the One-Dimensional Vlasov–Poisson Equations”. In: *SIAM Journal on Numerical Analysis* 21.1 (June 1984), pp. 52–76. ISSN: 0036-1429. DOI: 10.1137/0721003.

[38] R. Hockney and J. Eastwood. *Computer Simulation Using Particles*. CRC Press, Mar. 2021. ISBN: 978-1-4398-2205-0.

[39] C. Birdsall and A. Langdon. *Plasma Physics via Computer Simulation*. Series in Plasma Physics. Taylor & Francis, 2004. ISBN: 978-1-4822-6306-0.

[40] R. P. Wilhelm and M. Kirchhart. “An interpolating particle method for the Vlasov–Poisson equation”. In: *Journal of Computational Physics* 473 (2023), p. 111720. ISSN: 0021-9991. DOI: 10.1016/j.jcp.2022.111720.

[41] M. Evans and F. Harlow. “The Particle-In-Cell method for Hydrodynamic Calculations”. In: *Report LA-2139, Los Alamos Scientific laboratory of the university of California* (1957).

[42] G. H. Cottet and P. A. Raviart. “On particle-in-cell methods for the Vlasov-Poisson equations”. In: *Transport Theory and Statistical Physics* 15.1-2 (1986), pp. 1–31. DOI: 10.1080/00411458608210442.

[43] B. Wang, G. H. Miller and P. Colella. “A Particle-in-cell Method with Adaptive Phase-space Remapping for Kinetic Plasmas”. In: *SIAM J. Sci. Comput.* 33.6 (Dec. 2011), pp. 3509–3537. DOI: 10.1137/100811805.

[44] A. Myers, P. Colella and B. Straalen. “A 4th-Order Particle-in-Cell Method with Phase-Space Remapping for the Vlasov–Poisson Equation”. In: *SIAM Journal on Scientific Computing* 39.9 (Feb. 2016), B467–B485. ISSN: 1095–7197. DOI: 10.1137/16M105962X.

[45] J. Ameres. “Stochastic and Spectral Particle Methods for Plasma Physics”. PhD thesis. Technische Universität München, 2018.

[46] M. Kraus et al. “GEMPIC: geometric electromagnetic particle-in-cell methods”. In: *Journal of Plasma Physics* 83.4 (2017), p. 905830401. DOI: 10.1017/S002237781700040X.

[47] H. Bureau et al. “PIConGPU: A Fully Relativistic Particle-in-Cell Code for a GPU Cluster”. In: *IEEE Transactions on Plasma Science* 38.10 (2010), pp. 2831–2839. DOI: 10.1109/TPS.2010.2064310.

[48] S. Fasoulas et al. “Combining particle-in-cell and direct simulation Monte Carlo for the simulation of reactive plasma flows”. In: *Physics of Fluids* 31.7 (July 2019), p. 072006. ISSN: 1070-6631. DOI: 10.1063/1.5097638.

[49] J. Derouillat et al. “Smilei : A collaborative, open-source, multi-purpose particle-in-cell code for plasma simulation”. In: *Computer Physics Communications* 222 (2018), pp. 351–373. ISSN: 0010-4655. DOI: 10.1016/j.cpc.2017.09.024.

[50] L. Fedeli et al. “Pushing the Frontier in the Design of Laser-Based Electron Accelerators with Ground-breaking Mesh-Refined Particle-In-Cell Simulations on Exascale-Class Supercomputers”. In: *SC22: International Conference for High Performance Computing, Networking, Storage and Analysis*. 2022, pp. 1–12. DOI: 10.1109/SC41404.2022.00008.

[51] P. Parodi et al. “Pantera: A PIC-MCC-DSMC software for the simulation of rarefied gases and plasmas”. In: *SoftwareX* 31 (2025), p. 102244. ISSN: 2352-7110. DOI: 10.1016/j.softx.2025.102244.

[52] J. Brackbill and D. Forslund. “An implicit method for electromagnetic plasma simulation in two dimensions”. In: *Journal of Computational Physics* 46.2 (1982), pp. 271–308. ISSN: 0021-9991. DOI: 10.1016/0021-9991(82)90016-X.

[53] R. J. Mason. “Implicit moment particle simulation of plasmas”. In: *Journal of Computational Physics* 41.2 (1981), pp. 233–244. ISSN: 0021-9991. DOI: 10.1016/0021-9991(81)90094-2.

[54] G. Lapenta, J. Brackbill and P. Ricci. “Kinetic approach to microscopic-macroscopic coupling in space and laboratory plasmas”. In: *Physics of Plasmas* 13.5 (2006). DOI: 10.1063/1.2173623.

[55] S. Markidis, G. Lapenta and Rizwan-uddin. “Multi-scale simulations of plasma with iPIC3D”. In: *Mathematics and Computers in Simulation* 80.7 (2010). Multiscale modeling of moving interfaces in materials, pp. 1509–1519. ISSN: 0378-4754. DOI: 10.1016/j.matcom.2009.08.038.

[56] G. Lapenta. “Exactly energy conserving semi-implicit particle in cell formulation”. In: *Journal of Computational Physics* 334 (2017), pp. 349–366. ISSN: 0021-9991. DOI: 10.1016/j.jcp.2017.01.002.

[57] F. Bacchini. “RelSIM: A Relativistic Semi-implicit Method for Particle-in-cell Simulations”. In: *The Astrophysical Journal Supplement Series* 268.2 (2023). DOI: 10.3847/1538-4365/acefba.

[58] T. Arshad, Y. Chen and G. Tóth. “Adaptive mesh refinement in semi-implicit particle-in-cell method”. In: *Computer Physics Communications* 316 (2025), p. 109806. ISSN: 0010-4655. DOI: 10.1016/j.cpc.2025.109806.

[59] F. Bacchini, J. Amaya and G. Lapenta. “The relativistic implicit Particle-in-Cell method”. In: *Journal of Physics: Conference Series* 1225.1 (2019), p. 012011. DOI: 10.1088/1742-6596/1225/1/012011.

[60] J. Croonen et al. “An Exactly Energy-conserving Electromagnetic Particle-in-cell Method in Curvilinear Coordinates”. In: *The Astrophysical Journal Supplement Series* 271.2 (2024), p. 63. DOI: 10.3847/1538-4365/ad31a3.

[61] F. Filbet and E. Sonnendrücker. “Numerical methods for the Vlasov equation”. In: *Numerical Mathematics and Advanced Applications*. Milano: Springer Milan, 2003, pp. 459–468. ISBN: 978-88-470-2089-4.

[62] P. Krah et al. “A Characteristic Mapping Method for Vlasov-Poisson with Extreme Resolution Properties”. In: *Communications in Computational Physics* 35.4 (2023), 905 – 937. DOI: 10.4208/cicp.OA-2024-0012.

[63] M. Kirchhart and R. P. Wilhelm. “The Numerical Flow Iteration for the Vlasov–Poisson Equation”. In: *SIAM Journal on Scientific Computing* 46.3 (2024), A1972–A1997. DOI: 10.1137/23M154710X.

[64] R.-P. Wilhelm et al. “High fidelity simulations of the multi-species Vlasov equation in the electro-static, collisional-less limit”. In: *Plasma Physics and Controlled Fusion* 67.2 (2025), p. 025011. DOI: 10.1088/1361-6587/ad9fdb.

[65] J. E. Marsden and A. Weinstein. “The Hamiltonian structure of the Maxwell-Vlasov equations”. In: *Physica D: Nonlinear Phenomena* 4.3 (1982), pp. 394–406. ISSN: 0167-2789. DOI: 10.1016/0167-2789(82)90043-4.

[66] N. Crouseilles, L. Einkemmer and E. Faou. “Hamiltonian splitting for the Vlasov–Maxwell equations”. In: *Journal of Computational Physics* 283 (2015), pp. 224–240. ISSN: 0021-9991. DOI: 10.1016/j.jcp.2014.11.029.

[67] E. Hairer, G. Wanner and C. Lubich. *Geometric Numerical Integration. Structure-Preserving Algorithms for Ordinary Differential Equations*. 2nd ed. Springer Series in Computational Mathematics 31. Springer, 2006. ISBN: 3540306633.

[68] L. N. Trefethen and J. A. C. Weideman. “The Exponentially Convergent Trapezoidal Rule”. In: *SIAM Review* 56.3 (2014), pp. 385–458. DOI: 10.1137/130932132.

[69] R.-P. Wilhelm and K. Kormann. *Restarting the Numerical Flow Iteration through low rank tensor approximations*. 2025. DOI: 10.48550/arXiv.2509.08474. arXiv: 2509.08474 [math.NA]. URL: <https://arxiv.org/abs/2509.08474>.

[70] K. Kormann. “A Semi-Lagrangian Vlasov Solver in Tensor Train Format”. In: *SIAM Journal on Scientific Computing* 37.4 (2015), B613–B632. DOI: 10.1137/140971270.

[71] P. Krah et al. *A Hybrid Semi-Lagrangian Flow Mapping Approach for Kinetic Electrostatic Electron Non-linear (KEEN) Waves*. DOI: ....

[72] Y. Cheng et al. “Discontinuous Galerkin Methods for the Vlasov–Maxwell Equations”. In: *SIAM Journal on Numerical Analysis* 52.2 (2014), pp. 1017–1049. DOI: 10.1137/130915091.

[73] F. Bacchini and A. A. Philippov. “Fundamental, harmonic, and third-harmonic plasma emission from beam–plasma instabilities: a first-principles precursor for astrophysical radio bursts”. In: *Monthly Notices of the Royal Astronomical Society* 529.1 (Feb. 2024), pp. 169–177. ISSN: 0035-8711. DOI: 10.1093/mnras/stae521.

[74] L. Pezzini et al. “Fully Kinetic Simulations of Proton-beam-driven Instabilities from Parker Solar Probe Observations”. In: *The Astrophysical Journal* 975.1 (2024), p. 37. DOI: 10.3847/1538-4357/ad7465.

[75] A. Bret, L. Gremillet and M. E. Dieckmann. “Multidimensional electron beam-plasma instabilities in the relativistic regime”. In: *Physics of Plasmas* 17.12 (Dec. 2010), p. 120501. ISSN: 1070-664X. DOI: 10.1063/1.3514586.